Journal of Nuclear Materials 392 (2009) 552–567

Contents lists available at ScienceDirect

Journal of Nuclear Materials

journal homepage: www.elsevier.com/locate/jnucmat

Application of the GRAAL model to leaching experiments with SON68 nuclear glass in initially pure water

P. Frugier [a,*], T. Chave [b], S. Gin [a], J.-E. Lartigue [c]

[a] CEA Marcoule, DTCD/SECM/LCLT, BP 17171, 30207 Bagnols-sur-Cèze Cedex, France
[b] ICSM Site de Marcoule, DEN/MAR/ICSM/LSFC, UMR 5257, BP 17171, 30207 Bagnols-sur-Cèze Cedex, France
[c] CEA Cadarache, DEN/CAD/DTN/SMTM/LMTE, 13108 Saint-Paul-Lez-Durance Cedex, France

ARTICLE INFO

Article history:
Received 16 January 2009
Accepted 28 April 2009

ABSTRACT

Based on a review of the current state of knowledge concerning the aqueous alteration of SON68 nuclear glass we have proposed a mechanistic model, GRAAL (Glass Reactivity with Allowance for the Alteration Layer) [P. Frugier, S. Gin, Y. Minet, T. Chave, B. Bonin, N. Godon, J.E. Lartigue, P. Jollivet, A. Ayral, L. De Windt, G. Santarini, J. Nucl. Mater. 380 (2008) 8]. This article describes how the GRAAL model hypotheses are solved using a calculation code coupling chemistry and transport. The geochemical solution of this model combines three major phenomena: chemical equilibria in solution, water and ion transport by convection or diffusion, and element diffusion through the passivating reactive interphase. The model results are compared with experimental data for SON68 glass leached in initially pure water both in a closed system and in renewed media. The comparison shows the model very satisfactorily accounts for variations in the pH and the element concentrations in solution as a function of time, the glass surface area in contact with solution, and the solution renewal rate. This success is due to the fact that the diffusion of elements through the alteration gel is taken into account in the model. This mechanism cannot be disregarded under most experimental conditions — if only to predict the solution pH — and must therefore be an integral part of the geochemical model.

1. Introduction

R7T7 nuclear glass is presently used for the conditioning of radionuclides coming from the reprocessing of French PWR power plants spent fuel. R7T7 glass processing consists in melting at 1050 °C a mixture of aluminoborosilicate glass and calcine containing the radionuclides. The reference option in France for the management of vitrified high-level waste packages is geological repository (law dated 28 August 2006 [2]). It is based in particular on an assessment of the long-term behavior of the glass in contact with groundwater during the thousands of years necessary for decay of the radionuclides incorporated in the glass structure. Over time scales inaccessible to laboratory experimentation, and faced with the chemical complexity of the glass and its environment, modeling is the principal means of assessing the source term, i.e. the flow of radionuclides released from the glass over time. Although the source term depends on thermal, hydrological, mechanical, chemical, radiological and biological phenomena, coupling between chemical and hydraulic phenomena is the key issue for source term prediction.

The alteration mechanisms of SON68 glass (the inactive glass reference for R7T7) in initially pure water and the options chosen to model them were described in an article entitled 'SON68 nuclear glass dissolution kinetics: current state of knowledge and basis of the model GRAAL' [1]. This model aims to give a mechanistic description of the aqueous alteration of SON68 nuclear glass and to confirm the relevance of the simplified hypotheses of the models, based on experimental results, which are used for safety studies concerning waste disposal [3]. Several developments are necessary for this purpose, the first of which is to verify that the model is capable at laboratory scale of reproducing the effects of the *S*/*V* ratio (glass-surface-area-to-solution-volume-ratio) and solution flow rate on the glass alteration kinetics.

After reviewing the basic hypotheses of the model we describe how the HYTEC geochemical calculation code [4] is used to solve the equation system. The model predictions are then compared with a large body of experimental data. The data obtained in initially pure water at 90 °C are modeled in this article.

Recent reviews of the alteration mechanisms of glass in general [5–7] and of SON68 nuclear glass in particular [1] highlight the progress made toward understanding the phenomena involved. The key mechanisms of SON68 glass alteration are shown graphically in Fig. 1 and summarized below:

- Exchange and hydrolysis reactions involving the mobile glass constituents (alkalis, boron, etc.) occur rapidly during the initial instants.

* Corresponding author. Tel.: +33 466797724; fax: +33 466796620.
E-mail address: pierre.frugier@cea.fr (P. Frugier).

0022-3115/$ - see front matter © 2009 Elsevier B.V. All rights reserved.
doi:10.1016/j.jnucmat.2009.04.024

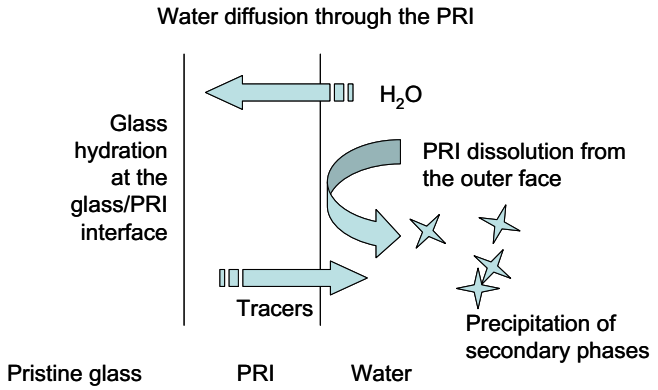

Fig. 1. Simplified diagram of the predominant mechanisms of SON68 glass alteration taken into account in the GRAAL model.

- Slower hydrolysis, especially of silicon, results in the existence of an initial glass dissolution rate.
- The difference between these two kinetics results in the creation of an amorphous layer at the glass/solution interface regardless of the alteration conditions. This layer is gradually reorganized by hydrolysis and condensation mechanisms [8,9].
- The amorphous layer dissolves as long as the solution is not saturated with respect to its constituent elements (Si, Zr, Al, Ca, etc.). Renewal of a pure water solution sustains the dissolution process.
- The amorphous layer constitutes a barrier against the transport of water toward the glass and of solvated glass ions into solution [10]. The existence of this transport-inhibiting effect rapidly causes this layer to control glass alteration. It is called 'passivating reactive interphase' (PRI) in accordance with its properties.
- Some glass constituent elements precipitate as crystallized secondary phases. The precipitation of these crystallized phases on the external surface or in solution can sustain glass alteration [11].

The principal simplifying hypotheses of the GRAAL model are the following.

- The amorphous layer can be schematically divided into several zones, each of which is associated with a key mechanism. The model describes only the PRI, which limits the diffusion of water and mobile elements, especially the alkalis and boron. As explained in [1], the other zones (glass hydration zone and gel zone depleted in network-forming elements) are not taken into account. Some authors refer to the PRI as a hydrated glass [12] or gel [13] depending on the importance they attribute to its being a residual solid (hydrated glass) or a recondensed solid (gel), but admittedly this solid is certainly formed by both mechanisms.
- A single apparent diffusion coefficient is used to simulate water diffusion in the PRI and diffusion of hydrolyzed and solvated glass constituent elements into solution.
- The reactivity of the PRI with the leaching solution is described by a thermodynamic equilibrium.

The equations in the GRAAL model and the solution to the chemistry-transport coupling are currently available in two forms.

- Analytical GRAAL: the first is an analytical solution with very simplified chemistry suitable for sensitivity calculations and for determining orders of magnitude. The equations used in this model are described in [1]. In this case only boron and silicon are specifically described; as a rough approximation the behavior of the mobile elements is thus considered comparable to boron, and that of the gel-forming elements comparable to silicon.
- Geochemical GRAAL: the second is a numerical solution using a geochemical calculation code. It provides a detailed chemical description (pH, speciation) in potentially complicated geometry (rough surfaces, crack network) and if necessary with materials other than glass.

This article details the geochemical solution to the equations derived from the hypotheses of the geochemical GRAAL model. The geochemical GRAAL model must meet two fundamental requirements:

- Accurately describe the chemistry with allowance for at least the major glass constituent elements as well as those supplied by the surrounding medium likely to have a significant impact on the glass alteration kinetics;
- Describe glass alteration in such a way as to allow coupled chemistry-transport calculations at the scale of a repository vault. The proposed glass model must therefore be easily interfaceable with modules describing the other nearfield materials.

Describing not only (1) the solution chemistry but also ion transport (2) in solution and (3) in the glass alteration film by means of a single model at each point in space and time is an extremely complex task. The existing models describe only one or two of these aspects simultaneously. Models based on Monte Carlo methods are designed to study morphological changes in the passivating reactive interphase, but the chemistry and transport of ions in solution are only taken into account in a very simplified manner [7,14]. Analytical models describe the surface layer but without allowance for chemistry and transport in solution provided by geochemical codes [15,12]. Geochemical models are suitable for a detailed description of chemistry and transport in solution, but generally do not take any account of reactive diffusion phenomena at the interfaces [16,17] — not because the latter are denied by their users [12,18], but simply because they are not formally taken into account: it is extremely complex to take all three mechanisms rigorously into account in a model for which the parameters are independent, limited in number, and measurable.

Nevertheless, these three key mechanisms and their coupling determine the glass alteration kinetics. This article describes a simple and effective manner of coupling transport phenomena at different scales (items 1 and 2) with the evolution of the chemical composition in solution (item 3). This approach does not only ensure that none of these mechanisms is neglected, but also allows for changes in their relative importance as a function of time, of the degree of confinement (high or low glass-surface-area-to-solution-volume ratio), and of the solution renewal rate.

2. Implementation of the geochemical GRAAL model

The geochemical version of the GRAAL model is based on the calculation hypotheses described in the following paragraphs.

Table 1
Simplified SON68 glass composition (oxide wt%). The selected elements represent 93.6 wt% (97 mol%) of the benchmark glass.

SiO_2	B_2O_3	Al_2O_3	Na_2O	Li_2O	CaO	Fe_2O_3	NiO	ZnO	P_2O_5	SrO	ZrO_2	MoO_3	Cs_2O
45.85	14.14	5.00	10.22	1.99	4.07	3.03	0.43	2.53	0.29	0.35	2.75	1.78	1.12

2.1. Glass composition

The model assumes a simplified glass composition (Table 1). The purpose is to account for the major glass constituent elements and the most soluble elements that can affect the pH and the speciation of other elements in solution. Increasing the number of elements taken into account would not raise any major difficulties if necessary, but this work was not done here.

2.2. Choice of amorphous phases described in the model

The geochemical GRAAL model simulates only the PRI, the amorphous zone formed in a closed system when the constituent element concentrations reach steady-state values in solution. This zone conserves the gel-forming elements (Si, Ca, Al, Zr etc.) as much as possible since their concentrations no longer increase in solution. Within the PRI there is a concentration gradient for the soluble elements (alkalis, B, Mo) and those having a strong affinity for crystallized phases (Zn, Ni, etc).

The decision to model only the PRI was based on the fact that the passivating properties attributed to it are significantly greater than for the depleted gel [19], but also because the material reserve constituted by the depleted gel appears to be negligible. This simplifying hypothesis will be tested, notably by the ability of the model to simulate experiments under flowing conditions.

2.3. Description of the passivating reactive interphase: thermodynamic or kinetic description?

The basic hypothesis is to describe the PRI as solid or a group of solids at thermodynamic equilibrium. The PRI is not considered as a thermodynamically stable solid, but its behavior is assumed comparable because its kinetic evolution toward more stable minerals is kinetically limited. Studies of natural or archaeological glass analogs have revealed the existence of very ancient gels [20,21]: their dissolution kinetic close to solution saturation is so low that a thermodynamic like steady state is obviously an efficient way for modeling their alteration.

2.4. PRI stoichiometry

Having postulated a thermodynamic description, the PRI must then be formally described. We chose the simplest option, which was to consider it as the sum of a number of separate simple phases: SiO_2, $Ca(OH)_2$, AlO(OH), and ZrO_2 were the chemical species selected for the formation of the PRI; they are the simple oxides or hydroxides precipitated by each element in aqueous solution. This approach has one significant limitation: it cannot take into account the chemical interactions between these elements in the gel. It is suitable, however, for identifying them before the development of a more powerful model precisely because it allows comparisons with the behavior of each element precipitating alone as a simple oxide or hydroxide. The relevance of this choice is discussed in detail in the section on the model limitations. The primary objective of this work is to propose a model coupling reactive diffusion with the dissolution reaction. This objective can be pursued relatively independently of the gel model, which has only a very moderate impact on the calculated altered glass thickness in initially pure water; this is not the case, however, when qualifying the reaction of the glass with the solids in the repository environment.

2.5. PRI thermodynamics

Assuming a thermodynamic description of the PRI as an assembly of simple oxide and hydroxide phases, the issue is to measure the solubility products associated with these phases to account for the steady-state concentrations in solution at equilibrium with the PRI.

The solubility products are determined from the equilibria indicated in Table 2. The reaction constants for two elements (expressed below) show that a pH-independent orthosilicic acid activity at saturation can reflect equilibrium with a single pure silica solid phase. They also show that the equation for silica is particularly simple, and that only the saturation indexes can qualify the saturation state of a solution in general.

$$SiO_2 = SiO_{2(aq)} \quad \log K_{eq1} = {}^{*}a_{SiO_{2(aq)}}$$

$$AlO(OH) = Al^{3+} + 2H_2O - 3H^+ \quad \log K_{eq2} = \frac{{}^{*}a_{Al^{3+}} {}^{*}a^2_{H_2O}}{{}^{*}a^3_{H^+}}$$

Using the CHESS [22] database, largely derived from the EQ3/6 code [23] database, variations in the steady-state activities of the various forms of dissolved silicon, aluminum and calcium were computed for extended experiments at 90 °C at high S/V ratios for which the preceding reactions very quickly reach steady-state conditions. For example, the data for experiments performed at S/V ratios of 80 and 2000 cm^{-1} (Table 5) are shown in Figs. 2–4. The precise conditions under which these experiments were

Table 2
Thermodynamic parameters and equations selected to describe the PRI.

Equations for the phase assembly selected to describe PRI	Log K at 90 °C
$SiO_2 = SiO_{2(aq)}$	2.910
$AlO(OH) = Al^{3+} + 2H_2O - 3H^+$	−4.245
$Ca(OH)_2 = Ca^{2+} + 2H_2O - 2H^+$	−13.506
$ZrO_2 = Zr^{4+} + 2H_2O - 4H^+$	4.998
$Sr(OH)_2 = Sr^{2+} + 2H_2O - 2H^+$	−22.762

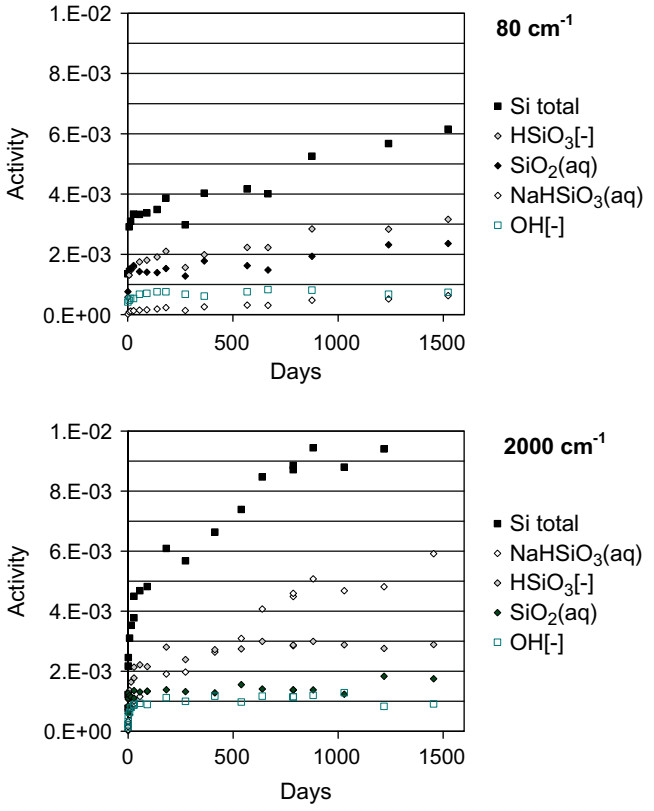

Fig. 2. Activities of silica species in experiments at 80 and 2000 cm^{-1}.

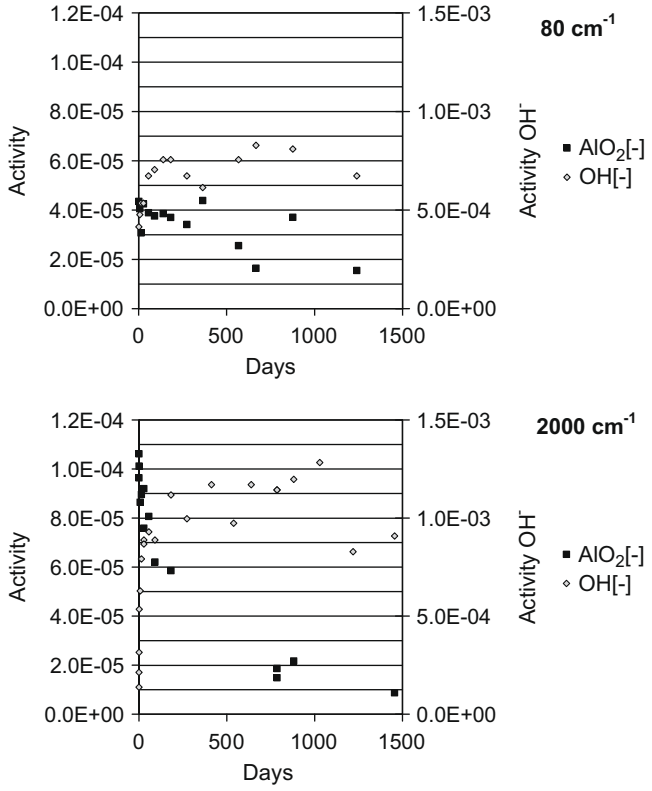

Fig. 3. Activities of major aluminum species in experiments at 80 and 2000 cm^{-1}.

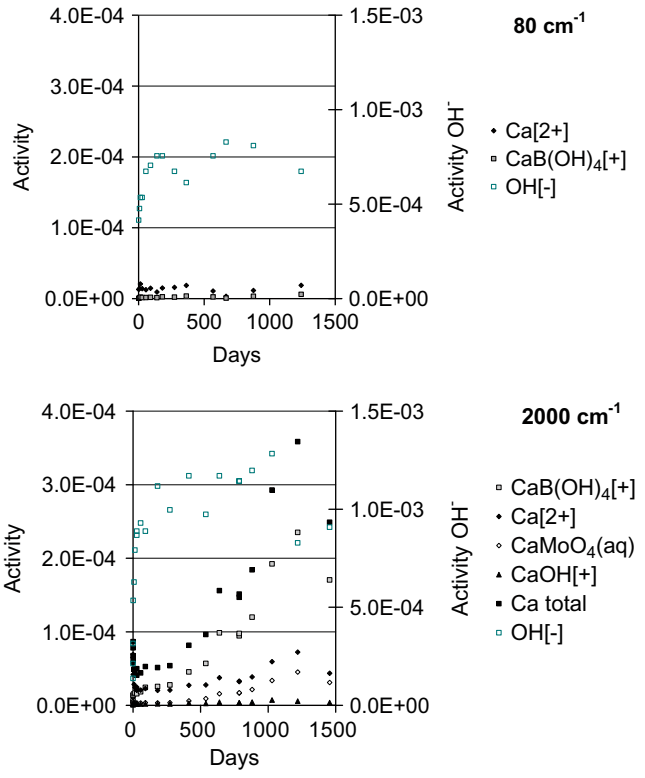

Fig. 4. Activities of calcium species in experiments at 80 and 2000 cm^{-1}.

carried out on powder samples are described in [24]. The 'equilibrium' pH values of the two experiments were comparable: 9.3 and 9.5, respectively, at 90 °C. The pH values calculated from electro-

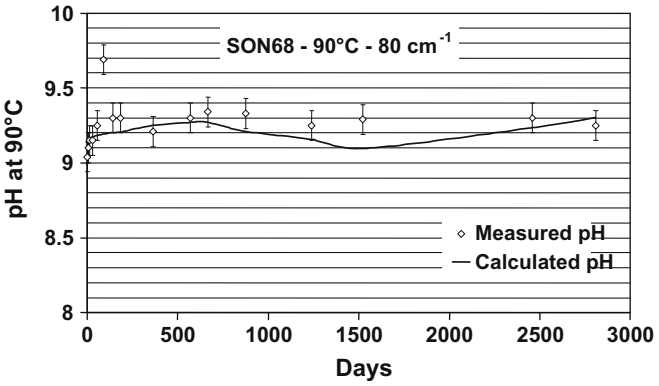

Fig. 5. Comparison between measured pH at 90 °C and pH recalculated via electroneutrality of solution: example of SON68 glass in initially pure water at 90 °C and 80 cm^{-1}.

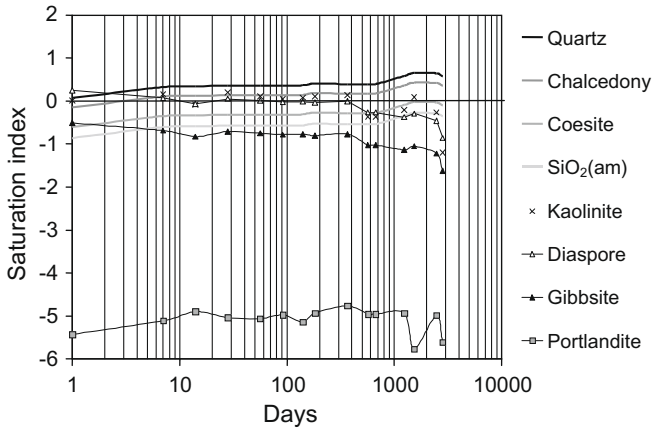

Fig. 6. Saturation indexes of a few simple phases: example of SON68 glass at 90 °C and 80 cm^{-1}.

neutrality of the assay solutions were consistent with the values measured experimentally (Fig. 5). The activities were recalculated using the measured pH. A CO_2 partial pressure of zero was assumed. Ionic activity coefficients were corrected with a truncated Davis equation. The objective here was not to model the experiments but simply to obtain a preliminary interpretation of the experimental data in terms of activity.

The calculations reveal several points.

- The H_4SiO_4 activity ($SiO_{2(aq)}$ in the figures) during these experiments in a closed system with initially pure water can be considered constant, irrespective of the *S*/*V* ratio and time (as a first approximation, allowing for the pH measurement uncertainty) at a value of about 2×10^{-3} at 90 °C. This is near the solubility of chalcedony (Fig. 6), as observed by [25].
- The rise in the total silicon concentration is attributable exclusively to the $NaHSiO_3$ complex that rapidly predominated at 2000 cm^{-1} and to the pH deviation ($HSiO_3^-$). This result shows that the silicon activity was controlled by a phase that dissolved to compensate for the appearance of the complex.
- The Ca^{2+} activity during these experiments in a closed system with initially pure water varied slightly with the S/V ratio and time, and was about 2×10^{-5} at pH 9 at 90 °C.
- The rise in the total calcium concentrations is attributable exclusively to the $CaB(OH)_4^+$ complex that rapidly predominated at 2000 cm^{-1}.

- The AlO_2^- activity at high S/V ratios appeared to decrease over time from 10^{-4} to 10^{-5}. This could be due to aluminum depletion from the gel phase to a crystallized phase.

The fact that the silicon activities are relatively independent of the S/V ratio and time shows that it is mathematically possible in these experiments to model silicon via the dissolution–condensation of a simple substance, SiO_2, which is consistent with Grambow's first model [26]. This does not mean that this approximation will still be valid in a reactive medium or for other solution or glass compositions. It is already known that the presence of aluminum and zirconium considerably diminishes the silicon activity at saturation, and that if these two elements are extracted from the PRI by another mechanism, the silicon alone will 'revert to' the solubility of amorphous silica [27]. Interactions between PRI constituents must be taken into consideration to account in detail for the reactivity of the passivating phase regardless of the gel composition.

The solubility of calcium hydroxide is very high and yet calcium exhibits a very strong affinity for silica gels in alkaline media [28]. The saturation indexes of portlandite are highly negative, although relatively constant for a given experiment at a given pH (Fig. 6). Portlandite appears less undersaturated at 2000 cm^{-1} and pH 9.5 (about 4 log) than at 80 cm^{-1} and pH 9.2 (about 5 log), indicating that a more complex interaction must be taken into account at least with silicon to correctly describe the calcium reactivity.

The aluminum behavior at the beginning of the experiments can be correctly described by assuming its solubility is near that of diaspore (Fig. 6). Over the long term the solution becomes undersaturated with respect to diaspore, which can be interpreted in two ways: either the selected phase is too simplistic, in which case using a Si–Al or Si–Ca–Al structure to describe PRI could account for this trend, or this behavior reflects the particular long-term reactivity of aluminum, which is stabilized not only in the PRI but also in the crystallized secondary phases.

Based on the preceding observations the PRI can be described using the values in Table 2. Zirconium is sparingly soluble and was not assayed; it is described by the solubility of zirconium oxide. Similarly, strontium hydroxide was selected to describe the solubility of strontium.

2.6. Rate law

The dissolution rate law for SON68 glass describing the progress of the glass hydration front is based on a PRI hydrolysis term, an affinity term for the equilibrium between the PRI and solution, and a term for diffusive ion transport in the PRI. The coupling between these terms is solved analytically in [1]. For the geochemical calculation, we chose not to formally solve the chemistry-transport coupling within the PRI, but to simplify it instead. The geochemical code already handles chemistry-transport coupling at macroscopic scale, although simultaneous management of microscopic and macroscopic coupling is not possible with the existing codes. The simplification necessary to mitigate this difficulty consists in not allowing for any feedback effect of the advancing glass hydration front on the ion diffusion rate in the PRI. The diffusion rate is entered directly in the code through a simple equation; its environmental dependence is limited to the effects of pH and temperature.

The selected rate law is the sum of the contributions of the following two terms:

$$V_{Hydr} = k_+[H^+]^n e^{\frac{-Ea}{RT}}\left(1 - \frac{a_{PRI}}{a^*_{PRI}}\right) \quad (1)$$

k_+ = initial rate (g m^{-2} d^{-1}); n = pH dependence coefficient of initial rate; Ea = apparent activation energy of initial rate (kJ mol^{-1}); a_{PRI} = PRI activity product; a^*_{PRI} = PRI activity product at saturation; R = ideal gas constant.

Table 3
Numerical values used for kinetic parameters in the rate law [29,30].

k_+	1.20×10^8	g m^{-2} d^{-1}
n	−0.40	dimensionless
Ea	76	kJ mol^{-1}
D_o	9.95×10^{-12}	m^2 s^{-1}
n'	−0.328	dimensionless
Ea'	83.5	kJ mol^{-1}

$$V_{diff} = \rho\left(\frac{D_0[OH^-]^{n'}e^{\frac{-E'a}{RT}}}{\pi t}\right)^{1/2} \quad (2)$$

ρ = glass density ($\rho = 2.76 \times 10^6$ g m^{-3}); D_0 = constant reactive diffusion coefficient (m^2 s^{-1}); n = coefficient of pOH^- dependence of reactive diffusion; Ea = apparent activation energy of reactive diffusion (kJ mol^{-1}).

The first term expresses the pH- and temperature-dependence of the initial PRI dissolution rate, and the exponential rate drop when the concentrations approach saturation of the PRI. This is a simple means of expressing the passivation of glass dissolution by the PRI. In the calculations shown here the PRI consists of several simple phases, but the a_{PRI} term of Eq (1) can only refer to a single phase. Silicon is the major constituent element, but also the most soluble in pure water; it is therefore reasonable at this stage of model development to designate the siliceous phase describing the PRI as controlling the overall glass alteration reaction. For these preliminary calculations in initially pure water, Eq. (1) identifies a first-order law for the siliceous phase resembling the comparable formalism proposed by [12].

The second term is the expression for the diffusion process versus the temperature and pH as proposed by [29] between 30 and 90 °C at pH 8–10. It corresponds to a mathematical formalism simulating ion diffusion through a PRI with a thickness that increases with the square root of time.

Table 3 summarizes the numerical values used for the kinetic parameters in the rate law. Note: the reactive diffusion rate calculated for a given time varies with the temperature according to an Arrhenius law in which the activation energy is equal to half that of the diffusion coefficient, i.e. $Ea'/2$ (see Eq. (2)). The reactive diffusion rate is thus less activated by the temperature than the PRI hydrolysis kinetics.

2.7. Additional issue

The fine powders used by Chave to configure the diffusion law were not in contact with aqueous solutions at any time prior to leaching [29]. As a result, in these experiments a small boron and alkali ion fraction was observed to enter solution almost instantaneously during the first few instants before the rate stabilized at a value proportional to the square root of time corresponding to the diffusion coefficient. This observation is consistent with the Monte Carlo models developed by Devreux et al. [14]: all the soluble atoms (boron, alkalis) initially present on the glass surface can be expected to enter solution extremely quickly. The surface must therefore be depleted in boron and alkali ions to a depth of a few atomic layers before any passivation effect can develop. The experimental data show that rapid initial reactivity must be assumed for the first six nanometers of the glass with unwashed powder. Instantaneous dissolution of 6 nm of glass was therefore added for all the simulations presented here, using the same powder samples as Chave. The instantaneous dissolution does not affect the concentration profiles in solution modeled for the experiments at $S/V < 500$ cm^{-1}, but cannot be disregarded for higher S/V values.

2.8. Crystallized mineral phases

Geochemical calculation code databases contain many mineral phases, but not all of them are likely to form at temperatures below 100 °C. Some can only be synthesized at high temperatures and have never been observed experimentally. They are largely supersaturated in the leaching solutions and taking them into account without any kinetic limitation in the calculations would result in extremely low element concentrations in solution. As we have opted for a purely thermodynamic database management, we must selectively consider only the mineral phases observed and the simple oxides and hydroxides whose precipitation at low temperatures has been established. The issue of taking into account phases capable of precipitating with slow kinetics must be raised for future predictive simulations. Table 4 indicates the mineral phases taken into account in the model for the experiments performed in pure water under oxidizing conditions. No kinetics are implemented for these phases. It may be noted that the phases selected in this model are not very different from those used by McGrail et al. [16] for other glass compositions.

Two phases not included in the CTDP database were added: sauconite $Na_{0.4}Zn_3Al_{0.4}Si_{3.6}O_{10}(OH)_2$ and pimelite $Ni_3Si_4O_{10}(OH)_2$. The data concerning their thermodynamic properties and stoichiometries are still incomplete. The log K values used for these phases only account for the low apparent solubility of zinc and nickel in solution. However the work by Chave [31] shows that they are necessary to account for the precipitation of nickel and zinc with a fraction of the silicon, sodium and aluminum from the glass.

Among the precipitating phases it is important to differentiate those with fast precipitation kinetics — for which the supply of a stoichiometric element from the glass or from the environment is a growth-limiting factor (Table 4) — from those with slow precipitation kinetics. Hydrated calcium silicates and zeolites were not taken into account in the calculations because they were not experimentally observed in the experiments described here.

The secondary minerals selected here are those suitable for describing the laboratory experiments performed in initially pure water under oxidizing conditions. In a complex chemical environment or under the reducing conditions expected in a geological repository, new phases must be considered.

2.9. Calculation code

The model has been implemented using the CHESS/HYTEC calculation code (versions 3.5 & 3.6) developed by the *École Nationale Supérieure des Mines de Paris* and uses the CTDP database [22].

3. Comparing the model with experimental data

We will demonstrate how the effects of the S/V and Q/S (solution flow rate/glass surface area) ratios can be modeled with a single parameter set. These two parameters were the main focus of research under the European GLAMOR Program [32]. We will consider the experiments carried out in initially pure water 90 °C; the effects of temperature, solution composition, and the presence of other materials in contact with the glass will be examined at a later date.

Table 5
Experiments performed on SON68 at 90 °C with different S/V ratios.

Experiment at increasing S/V	S/V (cm^{-1})	Source
1	3.3	P. Jollivet, personal communication (same protocol as Chave et al. [29])
2	80	Jegou [24]
3	200	Chave et al. [29]
4	2000	Gin et al. [33]

Table 6
Experiments performed on SON68 at 90 °C at different flow rates.

Experiment increasing Q/S	Q/S ($m\,d^{-1}$)	S/V (cm^{-1})	Solution renewal time in the reactor (days) = $(Q/S * S/V)^{-1}$
5	1.5×10^{-7}	4660	14.3
6	5.7×10^{-7}	2114	8.3
7	1.3×10^{-6}	4593	1.7
8	3.8×10^{-6}	1176	2.2
9	1.3×10^{-5}	823	0.9
10	4.9×10^{-5}	100	2.0
11	1.3×10^{-4}	85	0.9
12	5.1×10^{-4}	28	0.7

3.1. Experimental data studied

Table 5 lists the experiments carried out on SON68 glass in initially pure water at 90 °C in a closed system. Detailed descriptions of the experimental protocols can be found in the cited references.

Several experiments under flowing conditions initiated by Deneele for the GLAMOR project [32] are summarized in Table 6. The silicon and boron concentrations and the pH were measured at each sampling interval, providing a basis for comparison with the model.

3.2. Modeling results

Figs. 12–28 show the modeling results as variations over time in the concentrations of major elements dissolved in solution. Fig. 7 compares the simulated and experimental results based on the quantities of altered glass at the end of each of the twelve experiments.

Analyzing the results (refer to Appendix) leads to the following observations.

- Although the model uses a simple formalism with a limited number of parameters, it satisfactorily accounts for the element concentrations in solution. It describes variations of at least

Table 4
Mineral phases taken into account in the model (log K values from the CTDP database). No kinetics are implemented for these phases: they precipitate at saturation at the rate their constituent elements are supplied. The simple mineral phases (hydroxides, amorphous silica) are conserved for calculation purposes but are not listed, given the presence of more stable mineral phases.

Mineral	Dissolution equation	log K at 90 °C
Na nontronite	$Na_{0.33}Fe_2Al_{0.33}Si_{3.67}O_{10}(OH)_2 = 2\ Fe^{3+} + 0.33\ Na^+ + 0.33\ Al^{3+} + 3.67\ SiO_{2(aq)} + 4.66\ H_2O - 7.32\ H^+$	13.313
Hydroxylapatite	$Ca_5(PO_4)_3(OH) = 5\ Ca^{2+} + 3\ HPO_4^{2} + H_2O - 4H^+$	10.143
Powellite	$CaMoO_4 = Ca^{2+} + MoO_4^{2-}$	7.740
Sauconite	$Na_{0.4}Zn_3Al_{0.4}Si_{3.6}O_{10}(OH)_2 = 0.4\ Na^+ + 0.4\ Al^{3+} + 3\ Zn^{2+} + 3.6\ SiO_{2(aq)} + 4.8\ H_2O - 7.6\ H^+$	−20[a]
Pimelite	$Ni_3Si_4O_{10}(OH)_2 = 3\ Ni^{2+} + 4\ SiO_{2(aq)} + 4\ H_2O - 6\ H^+$	−10[a]

[a] Unknown values, arbitrarily fitted (they affect only the Zn^{2+} and Ni^{2+} activities, which are not discussed here).

three orders of magnitude in the altered glass quantities using only the parameter set described earlier. It is thus capable of describing the effects of the three main parameters: time, the S/V ratio, and the Q/S ratio.

- The predictive capabilities of the model are fully satisfactory compared with the experimental uncertainties: even though the best experimental protocols, for example Soxhlet, allow the rate to be measured within 20%, it is more difficult to carry out experiments under flowing conditions — especially to ensure complete stirring of a reactor containing a large quantity of powder, and to maintain a constant feed rate over extended time periods. Moreover, the data compiled here were obtained from different studies performed at different points in time on different powder batches and by different experimenters.

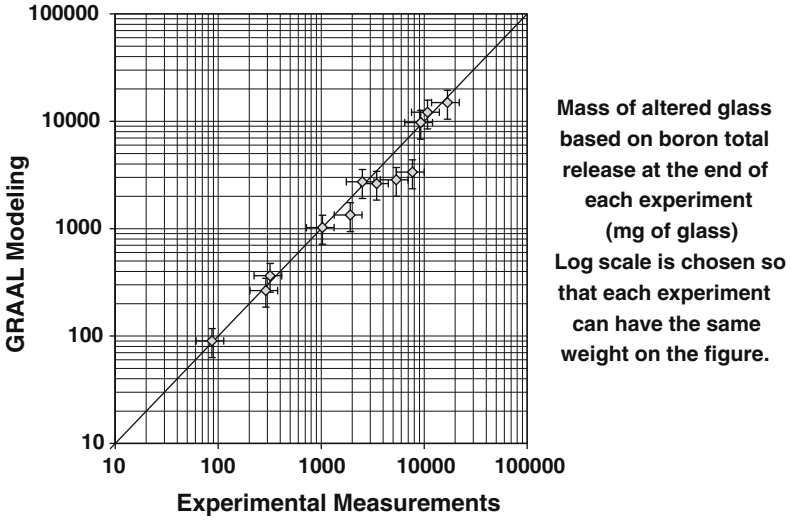

Fig. 7. Altered glass mass calculated by the model compared with experimentally measured values. Calculations were performed at the last sampling interval of each experiment. To identify their positions on the graph, the experiments are classified by order of increasing quantity of altered glass: 1, 12, 3, 11, 2, 10, 6, 9, 8, 4, 5, 7.

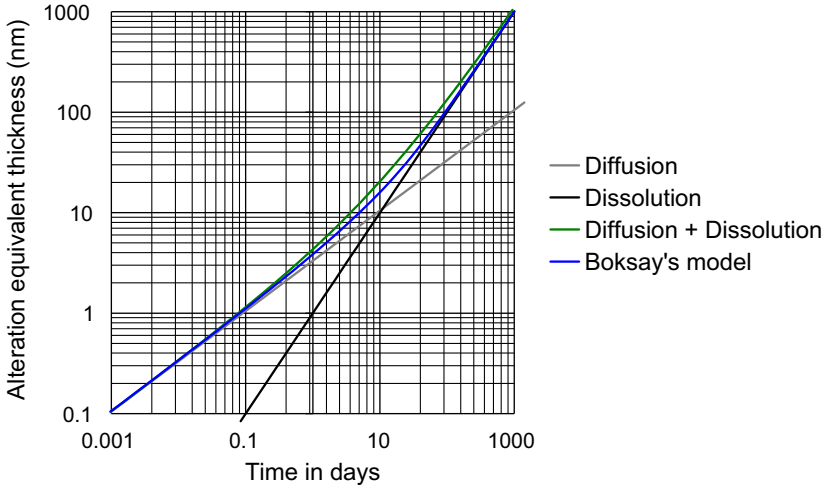

Fig. 8. Error generated by summing the diffusion and dissolution terms compared with the exact solution proposed by Boksay for a constant hydrolysis rate 'r'. The numerical application is for $D = 10^{-22}$ m^2 s^{-1} and $r = 10^{-3}$ μm d^{-1}. The numerical values affect only the scales; the relative positions of the curves are not value-dependent.

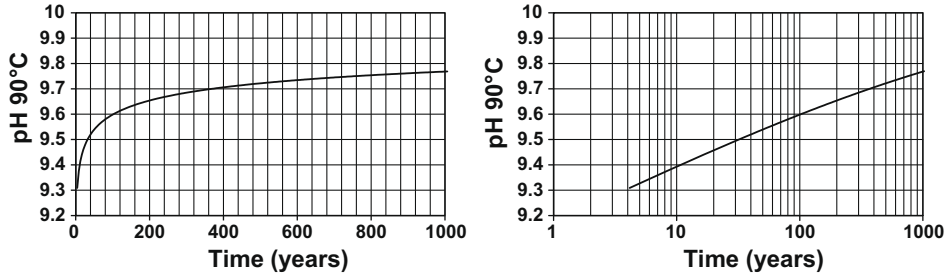

Fig. 9. Long-term pH predicted by the model for SON68 glass at 90 °C with an S/V ratio of 80 cm^{-1}.

Finally, the shape of the curves over time are satisfactorily reproduced, as is the incongruence between boron and silicon, reflecting the competition between diffusion and hydrolysis.

- The pH values are properly reproduced for all the experiments in open or closed systems (for example: Fig. 13). This was expected since the major element concentrations are correctly modeled.

Figs. 29–31 show the solids formed during leaching for three sets of representative experimental conditions.

- In a closed system at a high S/V ratio (Fig. 29), all the mineral phases form very quickly and their quantities vary with the square root of time. Ion diffusion within the PRI is the primary alteration mechanism; saturation is reached very quickly for all the phases at such a high S/V ratio (80 cm^{-1} is equivalent to a water thickness of only 125 μm on each glass surface). For SON68 glass, the complexation of orthosilicic acid by hydroxide ions or by sodium over time increases the dissolved silicon fraction but without significantly modifying the quantity of silica formed in the PRI, which continues to approximate a square root of time variation.
- At a lower S/V ratio the role of the hydrolysis process (dissolution of the PRI) becomes more important. At 3.3 cm^{-1} (Fig. 30) a month is necessary to reach saturation (equilibrium between the PRI and solution) and for diffusion to begin to increase in the PRI.
- In renewed media the diffusion term eventually always becomes negligible compared with the hydrolysis term, but at low flow rates per unit area the diffusion term predominates for several months. At 3.8×10^{-6} m d^{-1} (Fig. 24), for example, the quantity of silica formed in the PRI begins to diminish only after about 20 days because the flow of material arising from diffusion

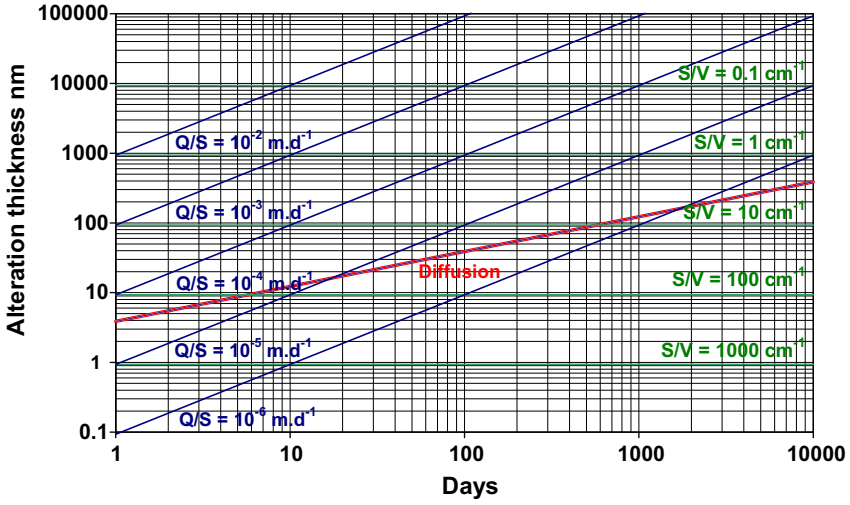

Fig. 10. Ranking of alteration drivers versus time for leaching of SON68 glass (simplified calculation without feedback, using the thermodynamic and kinetic parameters of leaching at pH 9 at 90 °C). The expected *altered glass thickness* is the sum of the contributions of each mechanism: reactive diffusion, the quantity of altered glass necessary to reach silicon saturation with respect to the PRI formed in a closed system depending on the S/V ratio, and the effect of solution renewal versus flow rate per unit area (Q/S). Example: For $S/V = 100$ cm^{-1} and $Q/S = 10^{-6}$ m d^{-1}, the diffusion mechanism predominates after 5 days of leaching, and the effect of solution renewal becomes significant only beyond 1000 days.

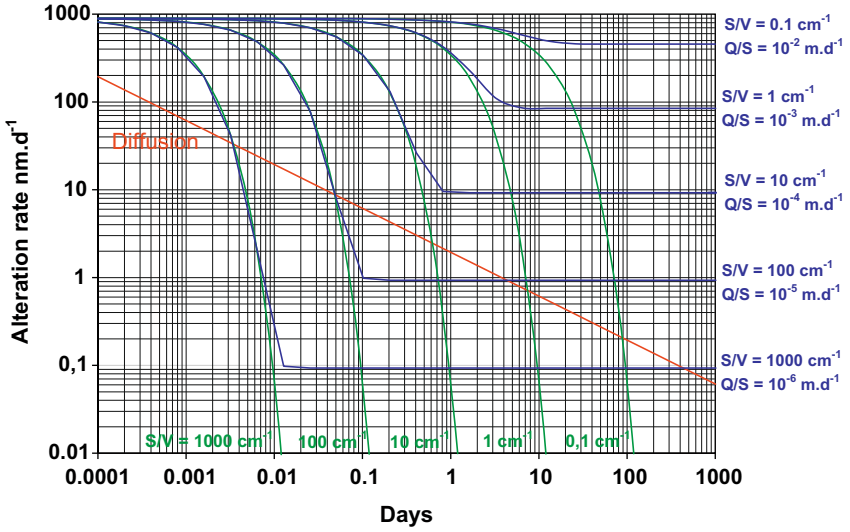

Fig. 11. Ranking of alteration drivers versus time for leaching of SON68 glass (simplified calculation without feedback, using the thermodynamic and kinetic parameters of leaching at pH 9 at 90 °C). The expected *alteration rate* is the sum of the contributions of each mechanism: reactive diffusion, the quantity of altered glass necessary to reach silicon saturation with respect to the PRI formed in a closed system depending on the S/V ratio, and the effect of solution renewal versus flow rate per unit area (Q/S).

(which diminishes with the square root of time) is equal to the flow supplied by solution renewal (which is constant in this case). After 4 months the silica will disappear from the PRI, and the overall glass dissolution will then be entirely controlled by the PRI hydrolysis kinetics. Note that although the PRI disappears in the simulation, this is not the case in reality: a very thin PRI layer of a few nanometers will remain; a precise thickness estimate can be obtained simply by applying Boksay's model [1,34].

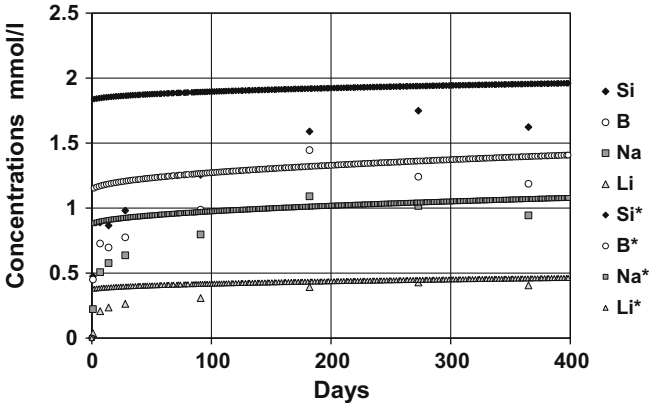

Fig. 12. SON68 glass, 90 °C, $S/V = 3.3\ cm^{-1}$. Remarks for Fig. 12: as expected, the alteration kinetics during the first few days were largely overestimated by not allowing for silicon retention in a gel that was less dense and less passivating than the gel that subsequently formed after a steady-state silicon concentration was reached. However, the final concentrations and their longer-term variation were well reproduced.

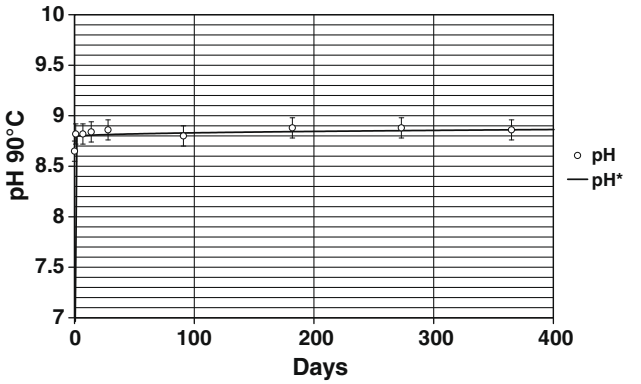

Fig. 13. SON68, 90 °C, $S/V = 3.3\ cm^{-1}$, pH measured at 90 °C and predicted pH.

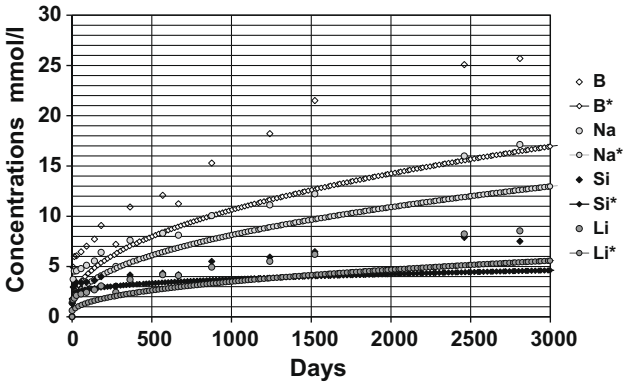

Fig. 14. SON68, 90 °C, $S/V = 80\ cm^{-1}$.

4. Discussion: limitations of the model

4.1. Operation equations

The reader might find it unsettling to see that from the standpoint of the code the two proposed laws, Eqs. (1) and (2), are applied to the entire pristine glass composition and generate apparently congruent dissolution, whereas the first corresponds to the PRI hydrolysis kinetics and the second concerns only the mobile elements. We shall demonstrate how these two laws are capable of accounting for the hypotheses of the GRAAL model.

The decision to model the PRI simply, based on thermodynamics alone, without kinetic parameters (see Section 2.3), implies that from the standpoint of the code only two situations are possible:

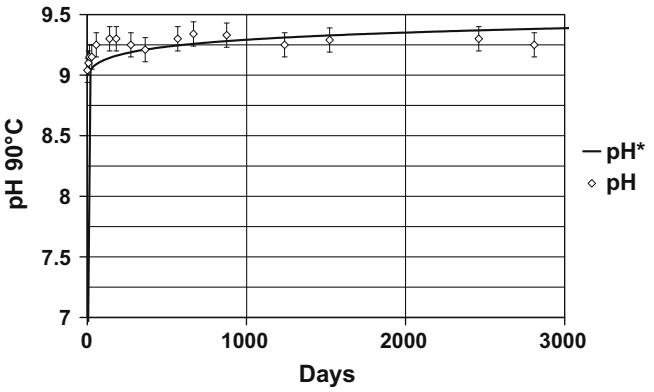

Fig. 15. SON68, 90 °C, $S/V = 80\ cm^{-1}$, pH measured at 90 °C and predicted pH.

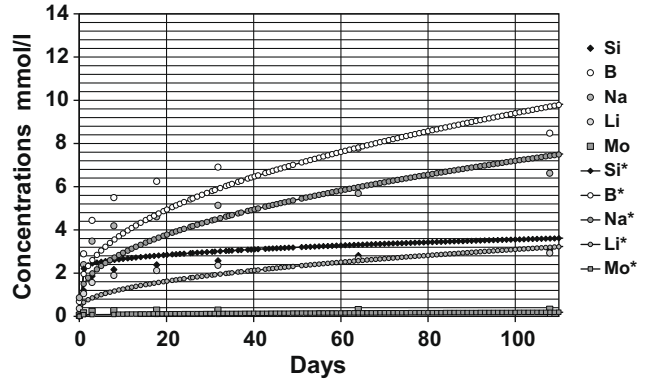

Fig. 16. SON68, 90 °C, $S/V = 200\ cm^{-1}$.

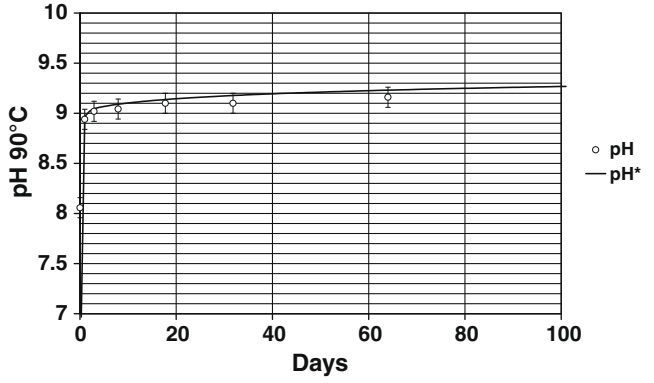

Fig. 17. SON68, 90 °C, $S/V = 200\ cm^{-1}$, pH measured at 90 °C and predicted pH.

either the solution is undersaturated with respect to the PRI (or more specifically compared with the constituent phases of the PRI) in which case the PRI does not form (case 1), or it is supersaturated, in which case it forms without any kinetic limitation (case 2). Let us consider these two possibilities in detail.

4.1.1. Case 1: initial rate conditions

Reactive diffusion, which is hard-coded in the rate law, is generated in the simplest possible way: by assuming a constant diffusion coefficient. Summing the hydrolysis and diffusion terms in the rate law implies that the dissolution and diffusion mechanisms are taken into account independently and in parallel. Summing these terms introduces a systematic error compared with a full coupling solution. The above hypothesis means that it is impossible to calculate the PRI thickness under initial rate conditions, contrary to the GRAAL analytical model or Boksay's model (refer to the following section).

Nevertheless, it is readily evident that:

- The calculation is numerically accurate in confined systems where diffusion predominates;
- The calculation is numerically accurate in renewed media where silicon removal is the predominant mechanism;
- The error generated in intermediate situations, compared with the theoretical model curve, overestimates the quantity of altered glass. The error is negligible because it concerns only transient conditions affecting nanometric thicknesses. Fig. 8 shows the error arising from this simplification.

The simplification was therefore implemented because the numerical application and the actual experiments show that under initial rate conditions the PRI thickness quickly becomes negligible compared with the total altered glass thickness. For example, an SON68 glass sample with an initial dissolution rate of 1 μm d^{-1} and a reactive dissolution coefficient of 10^{-22} m^2 s^{-1} will form an interdiffusion thickness of less than one nanometer within a few seconds (see [1] Fig. 2).

Depending on the formalism adopted, PRI dissolution does not affect the diffusion mechanism (except for the dependence of the

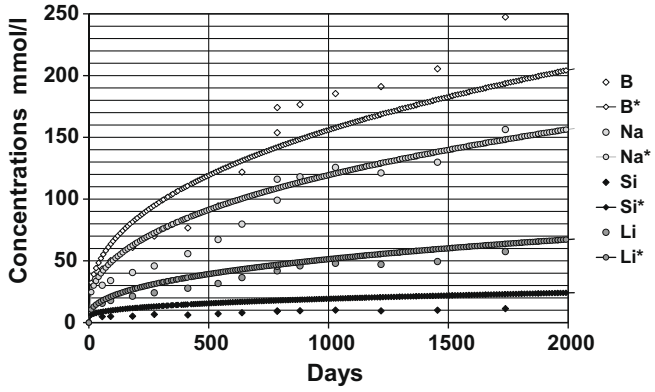

Fig. 18. SON68, 90 °C, $S/V = 2000$ cm^{-1}.

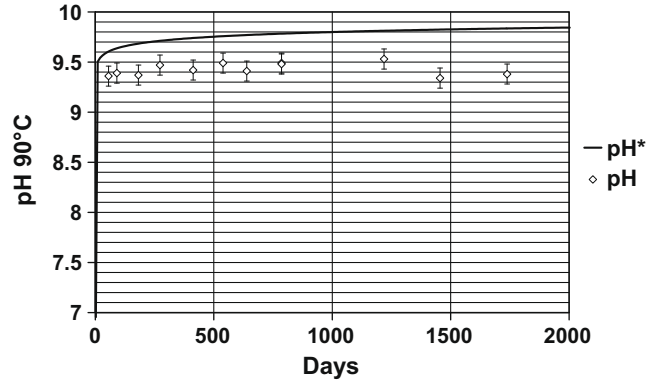

Fig. 19. SON68, 90 °C, $S/V = 2000$ cm^{-1}, pH measured at 90 °C and predicted pH.

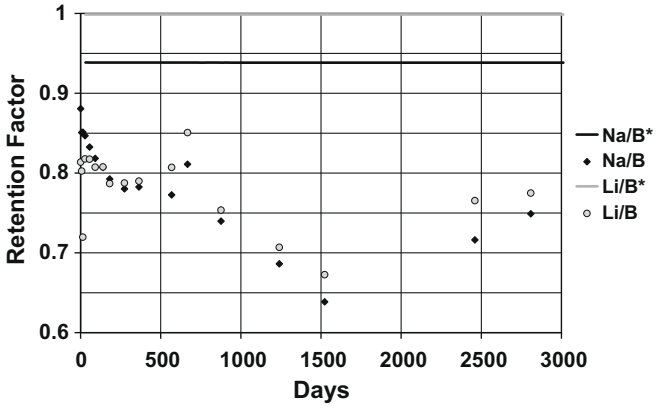

Fig. 20. Alkali/boron retention ratio: comparison between model and experiment at 2000 cm^{-1} at 90 °C.

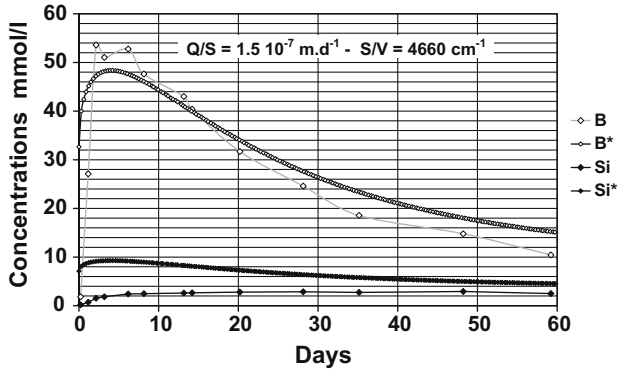

Fig. 21. SON68, 90 °C, $Q/S = 1.5 \times 10^{-7}$ m d^{-1}, $S/V = 4660$ cm^{-1}. Remarks for Fig. 21: As in Fig. 12, the silicon dissolution rate at the beginning of the experiments in Figs. 21–23 was overestimated by not allowing for silicon retention in a gel that was less dense and less passivating than the gel that subsequently formed after a steady-state silicon concentration was reached.

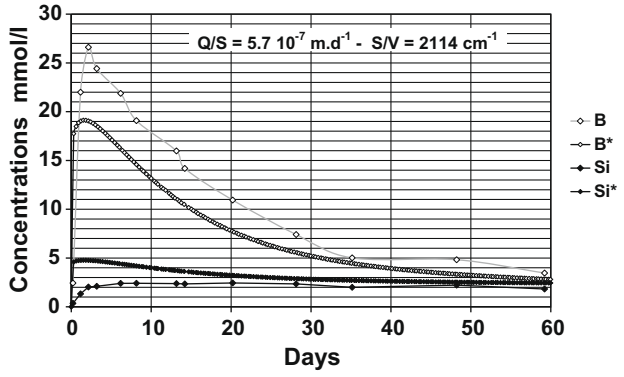

Fig. 22. SON68, 90 °C, $Q/S = 5.5 \times 10^{-7}$ m d^{-1}, $S/V = 2114$ cm^{-1}.

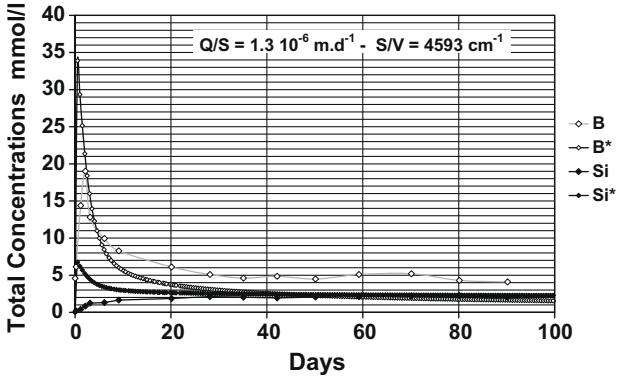

Fig. 23. SON68, 90 °C, $Q/S = 1.3 \times 10^{-6}$ m d^{-1}, $S/V = 4593$ cm^{-1}.

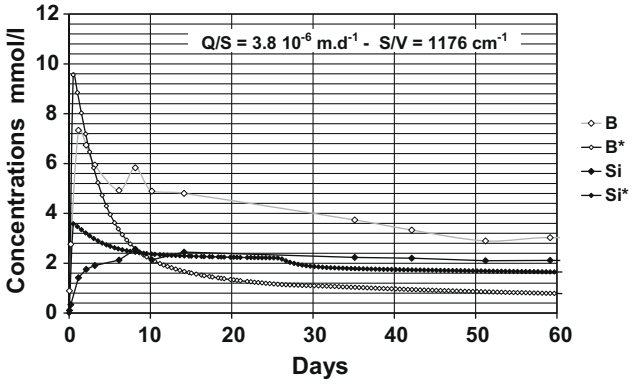

Fig. 24. SON68, 90 °C, $Q/S = 3.8 \times 10^{-6}$ m d^{-1}, $S/V = 1176$ cm^{-1}. Remarks for Fig. 24. It was more difficult to maintain a constant flow rate in this experiment than in the others. Leakage was observed repeatedly, and could account for the higher boron concentrations than predicted by the model, which assumed a constant flow rate.

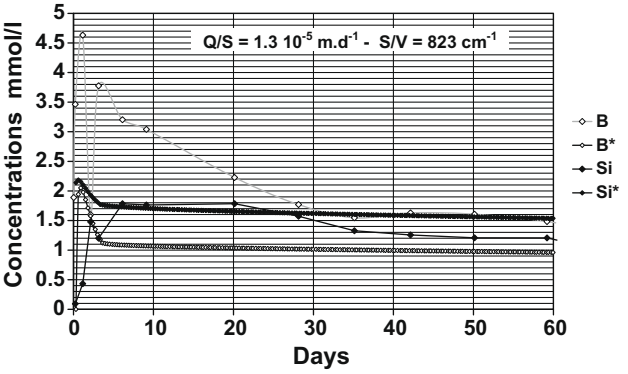

Fig. 25. SON68, 90 °C, $Q/S = 1.3 \times 10^{-5}$ m d^{-1}, $S/V = 823$ cm^{-1}.

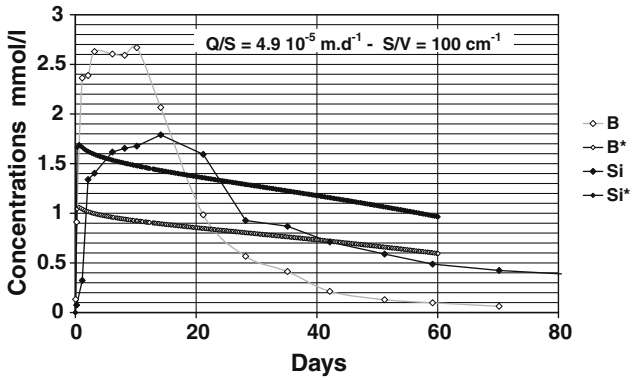

Fig. 26. SON68, 90 °C, $Q/S = 4.9 \times 10^{-5}$ m d^{-1}, $S/V = 100$ cm^{-1}.

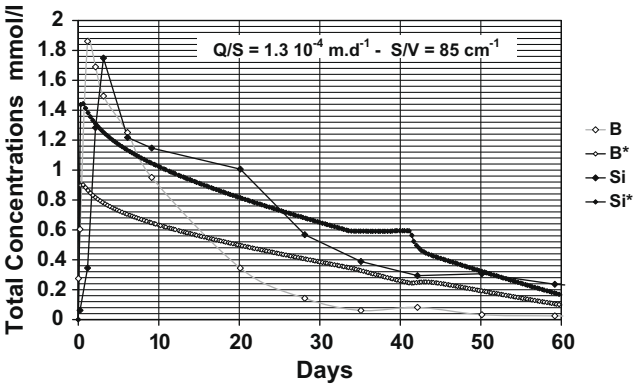

Fig. 27. SON68, 90 °C, $Q/S = 5.1 \times 10^{-4}$ m d^{-1}, $S/V = 28$ cm^{-1}.

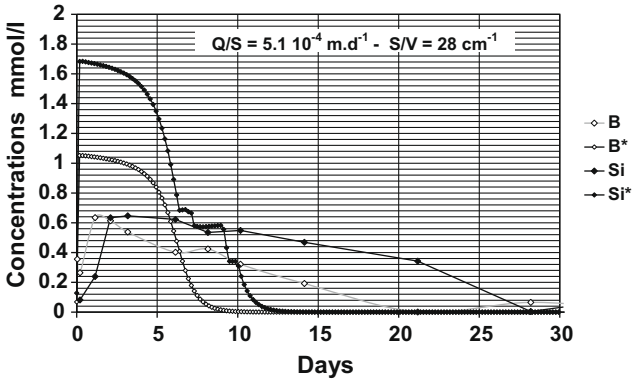

Fig. 28. SON68, 90 °C, $Q/S = 1.3 \times 10^{-4}$ m d^{-1}, $S/V = 85$ cm^{-1}.

diffusion coefficient on the solution pH). Moreover, taking into account a pH feedback effect on the diffusion process would be simplistic and mathematically false. As the pH changes, the entire shape of the diffusion profile in the solid is modified, not only the value of diffusion coefficient; the expression for the diffusion rate is therefore not strictly the same since the diffusion profile in the solid deviates somewhat from an error function [29]. Nevertheless, the impact of this modification is minor, and negligible compared with the experimental uncertainties. A more rigorous treatment of the diffusion process would involve a description of the concentration profiles at the interface for each computation time step. For example, this would make it possible to describe the effect of the advancing glass hydration front on the concentration profiles, or to determine the effect of a change in the pH — and thus in the diffusion coefficient — on the shape of the profile. In practice this is a difficult task, as changing the mesh scale (from ion diffusion over a few centimeters in water to a few nanometers in the PRI) raises significant numerical problems. Moreover, finite element models reach their limits at nanometric scale: molecular models will probably be required in this size range [7,14].

4.1.2. Case 2: 'saturation' conditions

In order to generate the overall incongruence observed by the experimenter analyzing the solution, the medium must be supersaturated with respect to the PRI. The incongruence is therefore related to the formation of the PRI — and of crystallized secondary

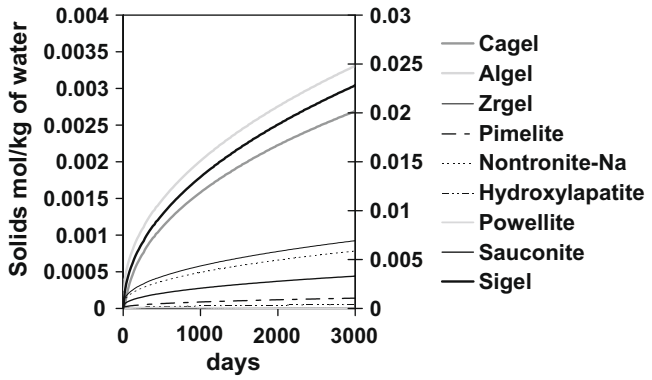

Fig. 29. Solids formed by SON68, 90 °C, $S/V = 80\ cm^{-1}$. Si_{gel}, which largely predominated, is shown on the right-hand scale.

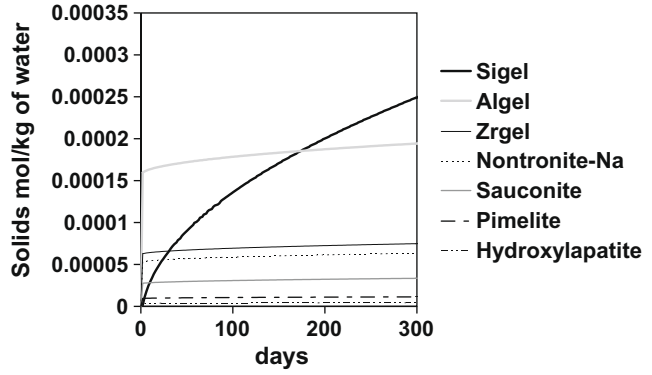

Fig. 30. Solids formed by SON68, 90 °C, $S/V = 3.3\ cm^{-1}$.

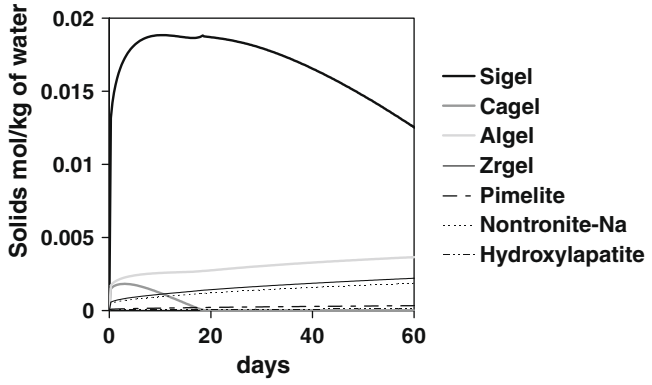

Fig. 31. Solid formed by SON68, 90 °C, $Q/S = 3.8 \times 10^{-6}\ m\ d^{-1}$, $S/V = 1176\ cm^{-1}$.

phases. Once saturation is reached, the diffusion law increases the mobile element concentrations in solution and produces increasing quantities of PRI and crystallized secondary phases. The diffusion law is thus indeed the driver behind incongruent dissolution.

The simple hypotheses and equations adopted here are sufficient to account for the experimental data. It is not indispensable for this purpose to formally describe the PRI in the code, which would require additional equations and distinct kinetic parameters. The model thus remains accessible and simple to use: this is an important point for investigating complex chemical systems and geometries. A more realistic treatment is nevertheless possible, provided the diffusion law is applied only to the elements actually concerned, but also if dissolution kinetics are applied to the PRI (in fact, the same as for the glass since it is a passivating phase) [30]. This more elegant approach is more difficult to implement and has no appreciable impact on the calculations. Finally, the hypothesis postulated to account for the complex reactive diffusion phenomena within the PRI using a single apparent diffusion coefficient certainly exceeds the mathematical precision of the solution (Fig. 8).

It should be noted here that this simplification is made possible simply by the fact that the PRI dissolution reaction diminishes exponentially as the medium approaches saturation, as shown by solving Eq. (1). The contribution of matter in solution due to the diffusion reaction thus quickly becomes negligible compared with that of the initial rate. However, it becomes predominant once saturation is reached in solution, given the exponential drop in the PRI dissolution reaction.

4.2. Modeling the PRI

Modeling the PRI in the form of simple phases does have limitations, but clearly reveals the necessity and potential contribution of taking account of chemical coupling in the PRI. Under the experimental conditions described here, with a single temperature, pH values near 9, and initially pure water, these synergistic effects are of the second order. Nevertheless, they determine the activities at saturation, especially for silicon, aluminum, and calcium. It is important to be able to predict them when accounting for composition effects in the glass and for predicting the precipitation of crystallized secondary mineral phases such as hydrated calcium silicates and zeolites.

Only the most passivating gel is modeled here. However, a fraction of the silicon condenses at H_4SiO_4 activities below the assumed saturation value — especially in particular locations such as near less soluble aluminum atoms [35]. A description of this gel with little or no passivating effect could certainly account for the fact that the silicon concentration modeled during the initial instants of experiments under flowing conditions exceeds the experimental value (Figs. 20–22).

A more detailed simulation of the PRI element activities in solution is essential, but will require a thorough reexamination of the PRI model, especially through a review of experimental data obtained with simplified glass compositions, and is therefore beyond the scope of this article. Nevertheless, the relative simplicity of diffusive transport as modeled here and its success in describing the boron and alkali concentrations will now allow us to consider modeling the PRI in detail.

4.3. Modeling crystallized secondary phases

Reactive diffusion of ions within the PRI modifies the pH and the activities of various elements. This raises the issue of the geochemical evolution of the system and especially the possible precipitation of new crystallized secondary phases over a time frame potentially inaccessible to experimentation. As demonstrated in [33], a constant residual rate is observed over the very long term at high S/V ratios (Figs. 14 and 18). This residual rate is not negligible compared with the rate of diffusion after more than one year of leaching, which until now has been modeled by adding a constant kinetic term [33]. The new modeling framework can take into account the precipitation of phases capable of maintaining a residual rate. The precipitation of a zeolite phase containing aluminum and sodium, or even a change in the smectite composition could explain not only the alkali retention (Fig. 20) but also the diminishing AlO_2^- activity over time (Fig. 3). Alkali retention is significant because not taking it into account in the model results in a pH overestimated by 0.3 units. Such precipitation has not been demonstrated experimentally, however, and is therefore not simulated for the moment.

Finally, the validity of the thermodynamic constants of pimelite and sauconite was not systematically verified, since nickel and zinc were rarely determined in the leachates. Nevertheless, this has no significant impact on the altered glass quantity. The secondary minerals selected here are those suitable for describing the laboratory experiments performed in initially pure water. In a complex chemical environment or under the reducing conditions expected in a geological repository, additional phases must be taken into consideration.

5. Using the model

5.1. Long-term pH variation

The pH is observed experimentally to increase with time and with the S/V ratio, and both these variations are correctly simulated. We can therefore use the model to extrapolate the solution pH value versus time and the S/V ratio. Fig. 9 shows the long-term pH variation if the assembly of secondary phases selected above remains unchanged.

The pH varies as a linear function of the logarithm of the product of $S/V \cdot t^{1/2}$. The modeled pH depends primarily on the (boron + molybdenum)/alkali concentration ratio, on the S/V ratio, on the time, and on the nature of the neoformed phases. Even in a closed system at a high S/V ratio over a long time period, SON68 glass alteration does not lead to high pH values at which rapid precipitation of zeolites has been observed to result in a resumption of alteration [36]. Slow precipitation of zeolites cannot be ruled out, as their saturation indexes (see the CTDP database) are positive in all the leaching solutions obtained during experiments at high S/V ratios. However, their precipitation consumes alkalis and significantly slows the pH rise (given the composition of SON68 glass), and thereby limits their tendency to crystallize quickly.

5.2. Preponderance of the various alteration drivers

Figs. 10 and 11 show the ranges in which the various alteration drivers predominate over time depending on the experimental conditions. Fig. 10 indicates the altered glass thickness values attributed to the diffusion mechanism, to the onset of saturation in the initially pure solution in contact with the glass (S/V), and to the effect of solution renewal (Q/S). The sum of these contributions determines the altered glass thickness. This simplified calculation illustrates the orders of magnitude and the predominant mechanism. The calculations shown here are based on the solubility parameters and diffusion coefficients adopted for a temperature of 90 °C and a pH of 9 at 90 °C. Contrary to the full model, no feedback is taken into account between the mechanisms, and for the pH variations in particular. Fig. 11 shows the same calculation expressed in terms of instantaneous rates. These schemes illustrate the importance of the effect of ion diffusion within the PRI on the concentrations of mobile elements (B, Na, Li, Mo), even at an S/V ratio of a few cm^{-1}. They show that diffusion cannot be disregarded in attempting to understand the geochemical evolution in a confined medium, such as a crack in a glass block, or a fractured glass block under geological repository conditions.

5.3. Brief comparison of GRAAL with the most recent models proposed for modelling SON68 glass dissolution

The main novelty between GRAAL and preceding models lie in the reactivity with the solution of the amorphous hydrated layer in which mobile elements gradients are observed. PRI may incorporate elements coming from solution even if they are not constituents of the glass. Such a mechanism seems not possible considering hydrated glass has defined by [12]. As a consequence geochemical GRAAL has been designed so that best effort could be put on the modeling of chemical reactions in the coming years. Nevertheless, analytical GRAAL is mathematically close to preceding BRAG model [37]: both models use a diffusion coefficient for mobile elements. Their authors both consider that more experimental data concerning water gradient within the alteration layer are required for justifying the explicit description of water diffusion as proposed in GM2001 model [12]. BRAG as GM2001 models take into account silica diffusion within the depleted gel. This last mechanism affects more silica than boron concentration in solutions. It is neglected in GRAAL because silica concentrations depends more on chemical than physical mechanisms as demonstrated in Fig. 2. Eventually, analytical GRAAL and BRAG model apparent diffusion coefficient for boron and alkali should have the same numerical value.

6. Conclusion

Modeling the effects of the glass-surface-area-to-solution-volume ratio (S/V) and of the flow rate per unit area (Q/S) when SON68 glass is leached in initially pure water has been a subject of considerable work in recent years, especially under the European GLAMOR Program [32]. Current models cannot account for the S/V effect without modifying their parameter values. This article has shown that by taking into account element speciation in solution, by reproducing the element distributions between crystallized secondary phases and the gel, and by allowing for ion diffusion in the passivating reactive interphase, a few simple hypotheses are sufficient to explain these effects with a single parameter set. The proposed model is designed to allow simple coupling of glass alteration with reactivity and transport in the complex chemical environment of a geological repository. It is also suitable for describing any composition effect involving the solution chemistry or the glass composition. Geochemical GRAAL is now validated whatever the S/V and Q/S ratios and the experiment geometry (for example a one scale glass block in a diffusive environment). Kinetic parameters and IRP and secondary phases solubility are given for initially pure water at 90 °C in a $pH_{90°C}$ range between 8 and 9.5. The range of these chemistry conditions will be soon extended.

7. Prospects

Future developments of the model are now being considered within the proposed framework. As mentioned in the experimental section, in addition to the effects of the S/V and Q/S ratios we must still confront our approach with the effects of temperature, solution composition, and leaching in contact with simple (e.g. iron) or complex (e.g. argillite) solids. The model is suitable for investigating the PRI — and especially the interactions between silicon, aluminum and calcium — notably by studying the effects of the glass composition. For example, the work reported in [25] merits reexamination after taking into account the diffusion mechanism in the PRI. Numerous perspectives exist for this approach in designing experiments and models of repository conditions or with complex geometries.

Acknowledgements

The authors are grateful to AREVA and the CEA for their financial support of this work. Special thanks are due to L. de Windt, J. Van der Lee and V. Lagneau of the *École Nationale Supérieure des Mines de Paris*, and to L. Trotignon and O. Bildstein of CEA Cadarache for further developing the functionality of chemistry-transport codes,

Table 7
Experimental conditions of leach tests.

Experiment	S/V (cm^{-1})	Q/S ($m\,d^{-1}$)	Powder size (μm)	BET sp. area ($m^2\,g^{-1}$)	Powder mass (g)	Initial pure water volume (mL)
1	3.3	0	63–125	0.0515	1.61	250.61
2	80	0	40–100	0.0968	24.790	300.0
3	200	0	Centered around 1.5	4.49	0.671	151.5
4	2000	0	5–40	0.581	51.660	150.8
5	4660	1.5×10^{-7}	Centered around 1.5	4.49	30.0045	289.0
6	2114	5.7×10^{-7}	Centered around 1.5	4.49	8.008	170.0
7	4593	1.3×10^{-6}	Centered around 5	1.39	100.076	302.0
8	1176	3.8×10^{-6}	Centered around 5	1.39	25.005	295.0
9	823	1.3×10^{-5}	Centered around 5	1.39	10.007	169.0
10	100	4.9×10^{-5}	Centered around 5	1.39	2.506	346.0
11	85	1.3×10^{-4}	Centered around 5	1.39	1.025	168.0
12	28	5.1×10^{-4}	Centered around 5	1.39	0.25	124

notably HYTEC, and the thermodynamic databases. We are also grateful to D. Deneele, P. Jollivet and C. Jégou of CEA Marcoule for allowing us to make use of their experimental data.

Appendix A. Experimental data

All the experiments described here were performed at 90 °C ± 2 °C in initially pure water (18.2 MΩ cm at 25 °C) in PTFE reactors of volumes ranging from 200 to 500 mL depending on the experiment. The powder mass was adjusted in each to obtain the desired S/V ratio according to the solution volume and the specific surface area of the powder. BET surface areas are used in this work, as distinct from the use of geometrical surface areas in short-term regulatory tests like PCT and MCC. The glass density was 2.8 kg L^{-1}. Slight evaporation of the leaching solutions was sometimes observed, but its effect on the concentrations and their evolution was negligible and is therefore not reported in the data tables. The variation of the S/V ratio over time resulting both from the reduction in the grain size and from solution sampling for analysis must be taken into account to compute accurate quantities of

Table 8
Experiment 1 (all concentrations are given in mmol L^{-1}).

pH 90 °C	Days	Si	B	Na	Li	Al	Ca	Mo
8.82	1	0.48	0.45	0.22	0.04	0.095	0.058	0.011
8.82	7	0.89	0.73	0.51	0.21	0.094	0.081	0.020
8.84	14	0.87	0.70	0.58	0.24	0.057	0.043	0.020
8.86	28	0.98	0.77	0.64	0.26	0.056	0.044	0.021
8.8	91	1.26	0.99	0.80	0.31	0.052	0.042	0.027
8.88	182	1.59	1.45	1.09	0.39	0.064	0.101	0.033
8.88	273	1.75	1.24	1.02	0.43	0.049	0.047	0.032
8.86	365	1.62	1.19	0.94	0.41	0.028	0.037	0.021
8.88	550	2.04	1.48	1.07	0.53	0.040	0.001	0.034

Table 9
Experiment 2 (all concentrations are given in mmol L^{-1}).

pH 90 °C	Days	Si	B	Na	Li	Al	Ca	Mo
9.04	1	1.35	1.78	1.39	0.62	0.045	0.017	X
9.10	7	2.95	4.93	3.74	1.70	0.043	0.021	X
9.15	14	3.16	5.99	4.54	1.85	0.033	0.032	X
9.15	28	3.40	6.07	4.57	2.13	0.045	0.022	X
9.25	56	3.41	6.47	4.79	2.27	0.042	0.020	X
9.69	91	3.47	7.03	5.12	2.43	0.040	0.024	X
9.30	140	3.60	7.73	5.55	2.68	0.042	0.016	X
9.30	182	4.00	9.08	6.40	3.06	0.040	0.026	X
9.25	274	3.06	7.21	5.01	2.44	0.037	0.026	X
9.21	364	4.16	10.92	7.61	3.70	0.048	0.033	X
9.30	568	4.34	12.08	8.31	4.18	0.028	0.020	X
9.34	667	4.18	11.24	8.11	4.10	0.018	0.006	X
9.33	876	5.51	15.29	10.07	4.94	0.041	0.023	X
9.3	1240	5.94	18.22	11.13	5.53	0.017	0.039	X
9.3	1523	6.48	21.51	12.23	6.21	0.018	0.008	X
9.3	2460	7.90	25.08	15.99	8.24	<0.017	<0.028	0.200
9.3	2809	7.51	25.70	17.13	8.54	<0.008	<0.005	0.169

Table 10
Experiment 3 (all concentrations are given in mmol L^{-1}).

pH 90 °C	Days	Si	B	Na	Li	Al	Ca	Mo
8.1	0.0	0.15	0.69	0.86	0.36	0.032	X	0.048
8.9	1.0	1.20	2.89	2.39	1.05	0.063	X	0.156
9.0	2.9	1.86	4.44	3.48	1.56	0.024	X	0.224
9.0	7.9	2.16	5.49	4.19	1.89	0.019	X	0.259
9.1	17.8	2.39	6.25	4.60	2.12	0.018	X	0.284
9.1	31.8	2.57	6.90	5.14	2.36	0.016	X	0.288
9.2	64.0	2.81	7.78	5.69	2.66	0.018	X	0.312
9.2	107.9	3.08	8.47	6.62	2.93	0.015	X	0.327

Table 11
Experiment 4 (all concentrations are given in mmol L^{-1}).

pH 90 °C	Days	Si	B	Na	Li	Al	Ca	Mo
9.4	56	4.83	43.38	30.20	15.65	0.090	0.066	0.840
9.4	91	5.06	50.14	34.03	17.89	0.097	0.071	0.880
9.4	182	5.20	60.92	40.56	21.33	0.076	0.087	0.948
9.5	273	6.63	70.04	45.84	24.15	0.072	0.085	1.040
9.4	413	6.15	76.68	55.81	27.81	0.004	0.090	1.129
9.5	539	7.22	94.48	67.26	31.69	0.004	0.136	1.545
9.4	639	8.01	121.88	79.73	36.44	0.004	0.159	2.390
9.5	786	9.20	153.78	99.04	41.88	0.004	0.255	3.259
9.5	786	9.42	174.10	116.02	45.58	0.025	0.239	4.150
X	881	9.57	176.54	118.05	45.91	0.020	0.246	4.215
X	1029	10.17	185.44	125.61	48.01	0.029	0.299	4.574
9.5	1219	9.53	191.05	121.13	47.08	0.004	0.472	4.691
9.3	1455	10.06	205.56	129.86	49.41	0.004	0.580	5.199
9.4	1738	11.30	247.38	156.33	57.49	0.012	0.398	6.106
9.4	2107	12.13	280.98	171.33	63.65	0.004	0.327	7.174
9.4	2310	13.57	388.95	249.01	83.98	0.017	0.688	10.513
9.4	3023	13.36	386.30	281.69	89.73	0.008	0.487	11.080

Table 12
Experiment 5 (all concentrations are given in mmol L^{-1}).

Days	pH 90 °C	Si	B
0.21	8.57	0.20	1.83
1.16	9.17	0.70	27.10
2.15	9.35	1.54	53.58
3.18	9.47	1.83	51.03
6.17	9.55	2.42	52.77
8.16	9.61	2.48	47.61
13.17	9.64	2.59	43.01
14.20	9.64	2.64	40.40
20.20	9.74	2.80	31.69
28.14	9.82	2.87	24.59
35.15	9.75	2.74	18.56
48.22	9.74	2.92	14.78
59.22	X	2.50	10.44

Table 13
Experiment 6 (all concentrations are given in mmol L^{-1}).

Days	pH 90 °C	Si	B
0.21	8.61	0.35	2.43
1.16	9.37	1.32	21.99
2.15	9.44	2.02	26.60
3.18	9.54	2.11	24.41
6.17	9.58	2.40	21.88
8.16	9.64	2.41	19.08
13.17	9.62	2.38	15.98
14.20	9.62	2.35	14.19
20.20	9.72	2.45	10.94
28.14	9.77	2.35	7.41
35.15	9.67	2.00	5.02
48.22	9.63	2.22	4.82
59.22	X	1.82	3.45

Table 14
Experiment 7 (all concentrations are given in mmol L^{-1}).

Days	pH 90 °C	Si	B
0.03	X	0.20	4.59
0.22	9.01	0.38	6.12
1.16	9.41	0.84	14.38
2.14	9.56	1.23	19.01
3.14	9.15	1.31	12.81
6.13	9.85	1.65	9.94
9.12	9.82	1.86	8.28
20.13	9.86	2.12	6.10
28.14	9.89	2.03	5.09
35.12	9.90	1.94	4.62
42.14	9.84	2.07	4.85
50.14	9.88	2.12	4.49
59.20	9.88	2.21	5.09
70.14	9.72	2.26	5.19
80.14	9.79	2.04	4.30
90.18	9.81	1.99	4.10

Table 15
Experiment 8 (all concentrations are given in mmol L^{-1}).

Days	pH 90 °C	Si	B
0.04	8.30	0.11	0.89
0.21	9.10	0.34	2.76
1.15	9.63	1.42	7.34
2.10	9.73	1.76	6.74
3.17	9.82	1.91	5.94
6.14	9.86	2.13	4.92
8.15	9.87	2.56	5.83
10.18	9.78	2.14	4.89
14.14	9.79	2.45	4.80
21.18	9.96	2.27	14.58
28.20	9.69	2.27	3.92
35.13	9.78	2.23	3.73
42.14	9.74	2.20	3.33
51.21	9.67	2.10	2.89
59.17	9.67	2.11	3.03
70.18	8.61	2.09	2.83

altered glass. This calculation was performed, and showed that assuming a constant S/V ratio during the tests generally provides a satisfactory result. In order to simplify this Appendix, only the element concentrations are indicated in Tables 7–19. The pH was measured at 90 °C and the analyzed concentrations are expressed in mmol L^{-1}. 'X' means that the relevant analysis was not carried out.

Uncertainties: The mean uncertainty values of the tests in the tables below are the following.

- Determination of major elements in solution: <5%.

Table 16
Experiment 9 (all concentrations are given in mmol L^{-1}).

Days	pH 90 °C	Si	B
0.03	8.77	0.09	1.89
0.22	9.10	0.43	3.46
1.16	9.63	1.48	4.63
2.14	9.54	1.20	1.60
3.14	9.19	1.78	3.78
6.13	9.78	1.76	3.20
9.12	9.70	1.78	3.04
20.13	9.60	1.57	2.23
28.14	9.56	1.33	1.77
35.12	9.56	1.25	1.55
42.14	9.60	1.21	1.63
50.14	9.60	1.21	1.61
59.20	9.65	0.88	1.48
70.14	9.58	1.06	1.25
80.14	9.56	1.23	1.34
90.92	9.55	1.08	1.29

Table 17
Experiment 10 (all concentrations are given in mmol L^{-1}).

Days	pH 90 °C	Si	B
0.04	X	0.07	0.13
0.21	7.90	0.32	0.91
1.15	9.00	1.34	2.36
2.10	9.64	1.40	2.39
3.17	9.69	1.62	2.63
6.14	9.71	1.65	2.60
8.15	9.72	1.68	2.59
10.18	9.68	1.79	2.67
14.14	9.63	1.59	2.07
21.18	9.52	0.93	0.98
28.20	9.37	0.87	0.57
35.13	9.45	0.71	0.41
42.14	9.19	0.59	0.21
51.21	8.99	0.49	0.13
59.16	8.94	0.42	0.10
70.18	9.67	0.35	0.06

Table 18
Experiment 11 (all concentrations are given in mmol L^{-1}).

Days	pH 90 °C	Si	B
0.03	8.37	0.06	0.27
0.22	9.04	0.35	0.60
1.16	9.56	1.28	1.86
2.14	9.70	1.75	1.69
3.14	9.06	1.22	1.49
6.13	9.59	1.15	1.25
9.12	9.50	1.01	0.95
20.13	9.34	0.57	0.34
28.14	9.12	0.39	0.14
35.12	9.01	0.29	0.06
42.14	8.80	0.31	0.08
50.14	8.48	0.24	0.03
59.20	8.55	0.19	0.02
70.14	8.18	0.15	0.02
80.14	7.91	0.10	0.02
90.18	6.86	0.09	0.01

- BET measurements of specific surface area: <10%. Allowance must be made for the relatively high uncertainty on the possible presence of very fine residual glass particles affecting the BET measurement.
- Initial S/V ratio: <10%. The ratio varied during each test, however, given the diminishing grain size and the volume of the solution samples taken for analysis. These variations were less than 20% for the tests in a closed system and for experiments 5–10, and 100% (disappearance of the glass grains) at the end of experiment 12.

Table 19
Experiment 12 (all concentrations are given in mmol L^{-1}).

Days	pH 90 °C	Si	B
0.04	7.50	0.08	0.36
0.21	9.00	0.24	0.26
1.15	9.42	0.63	0.63
2.10	9.41	0.65	0.61
3.17	9.45	0.62	0.54
6.14	9.39	0.54	0.40
8.15	9.41	0.55	0.42
10.18	9.29	0.47	0.32
14.14	9.05	0.34	0.19
28.20	8.39	0.107	0.065
35.13	6.50	0.062	0.016
42.14	6.77	0.031	0.014
51.21	6.29	0.019	0.017
59.17	7.01	0.011	0.014
70.18	7.06	0.011	0.012

- Q/S ratio: <15% allowing for flow rate variations during the test.
- Overall uncertainty on the altered glass thickness measurements: considering the uncertainties mentioned above and the experience acquired in the laboratory on the repeatability of experiments with different crushed glass batches, an uncertainty of less than 30% is applicable to all the tests.

References

[1] P. Frugier, S. Gin, Y. Minet, T. Chave, B. Bonin, N. Godon, J.E. Lartigue, P. Jollivet, A. Ayral, L. De Windt, G. Santarini, J. Nucl. Mater. 380 (2008) 8.
[2] Assemblée Nationale, Projet de loi de programme relatif à la gestion durable des matières et des déchets radioactifs, in: 590 ed., 2006, p. 1.
[3] I. Ribet, N. Godon, S. Gin, Y. Minet, P. Jollivet, P. Frugier, E. Vernaz, J.M. Cavedon, V. Petitjean, The V_0-V_t operational model for the long-term behavior of vitrified R7T7 waste packages, in: Advances for Future Nuclear Fuel Cycles Nimes, Atalante France, 2004, p. 1.
[4] J. van der Lee, L. De Windt, V. Lagneau, P. Goblet, Comput. Geosci. 29 (2003) 265.
[5] R. Conradt, J. Am. Ceram. Soc. 91 (2008) 728.
[6] S. Gin, C. Jegou, P. Frugier, Y. Minet, Chem. Geol. 255 (2008) 14.
[7] L. Zhang, A. Lüttge, J. Phys. Chem. B 112 (2008) 1736.
[8] M. Arab, C. Cailleteau, F. Angeli, F. Devreux, Experimental study and Monte Carlo modeling of calcium borosilicate glasses leaching, in: D. Dunn, C. Poinssot, B. Begg (Eds.), Scientific Basis for Nuclear Waste Management XXX, 985 ed., Materials Research Society, Boston, Massachussetts, USA, 2007, p. 193.
[9] A. Ledieu, F. Devreux, P. Barboux, Y. Minet, Nucl. Sci. Eng. 153 (2006) 285.
[10] C. Cailleteau, F. Angeli, F. Devreux, S. Gin, J. Jestin, P. Jollivet, O. Spalla, Nature Mater., in press.
[11] P. Frugier, C. Martin, I. Ribet, T. Advocat, S. Gin, J. Nucl. Mater. 346 (2005) 194.
[12] B. Grambow, R. Muller, J. Nucl. Mater. 298 (2001) 112.
[13] O. Spalla, P. Barboux, L. Sicard, S. Lyonnard, F. Bley, J. Non-Cryst. Solids 347 (2004) 56.
[14] F. Devreux, A. Ledieu, P. Barboux, Y. Minet, J. Non-Cryst. Solids (2003) 1.
[15] I. Ribet, S. Gin, E. Vernaz, R. Do Quang, Long-term behavior of nuclear glass: the $r(t)$ operational model, in: GLOBAL 2001, Paris, 2001, p. 1.
[16] B.P. McGrail, D.H. Bacon, J. Icenhower, F.M. Mann, R.J. Puigh, H.T. Schaef, S.V. Mattigod, J. Nucl. Mater. 298 (2001) 95.
[17] I. Munier, J.L. Crovisier, B. Grambow, B. Fritz, A. Clément, J. Nucl. Mater. 324 (2004) 97.
[18] B.P. McGrail, J. Icenhower, J.G. Darab, D.K. Shuh, D.R. Baer, V. Shutthanandan, S. Thevuthasan, G. Engelhard, J.L. Steele, E.A. Rodriguez, P. Liu, K.E. Ivanov, C.H. Booth, P. Nachimuthu, Ion-Exchange Processes and Mechanisms in Glasses, Pacific Northwest Laboratory (Ed.), 2001, p. 1.
[19] N. Valle, J. Sterpenich, G. Libourel, Geochim. Cosmochim. Acta (2001) 1.
[20] I. Techer, T. Advocat, J. Lancelot, J.M. Liotard, Chem. Geol. 176 (2001) 235.
[21] A. Verney-Carron, S. Gin, G. Libourel, Geochim. Cosmochim. Acta 72 (2008) 5372.
[22] J. van der Lee, L. De Windt, Chess tutorial and cookbook, Updated for version 3.0, in: École des Mines de Paris (Ed.), LHM/RD/02/13 ed., 2002.
[23] T.J. Wolery, A software package for geochemical modelling of aqueous systems: package overview and installation guide (version 7.0), in: Lawrence Livermore National Laboratory (USA) (Ed.), UCRL-MA-110662 ed., 1992.
[24] C. Jégou, S. Gin, F. Larché, J. Nucl. Mater. 280 (2000) 216.
[25] I. Munier, B. Grambow, B. Fritz, A. Clement, J. Nucl. Mater. 324 (2004) 97.
[26] B. Grambow, Am. Ceram. Soc. (1984) 474.
[27] S. Ribet, S. Gin, J. Nucl. Mater. 324 (2004) 152.
[28] L. Armelao, A. Bassan, R. Bertoncello, G. Biscontin, S. Daolio, A. Glisenti, J. Cult. Heritage 1 (2000) 375.
[29] T. Chave, P. Frugier, A. Ayral, S. Gin, J. Nucl. Mater. 362 (2007) 466.
[30] G. de Combarieu, Altération du verre de confinement de déchets type R7T7 en condition de stockage géologique. Ph.D. Thesis, Univ. Paris XI, Orsay, France, p. 1.
[31] T. Chave, Etude des mécanismes d'altération par l'eau du verre R7T7 en milieu confiné, compréhension et modélisation de la cinétique résiduelle, in: Université Montpellier II, Science et Technique du Languedoc, 2008, p. 1.
[32] P. Van Iseghem, M. Aertsens, S. Gin, D. Deneele, B. Grambow, P. McGrail, D. Strachan, G. Wicks, A critical evaluation of the dissolution mechanisms of high-level waste glasses in conditions of relevance for geological disposal (GLAMOR), in: SCK·CEN, CEA, Subatech, PNNL, SRNL (Eds.), EUR 23097 ed., 2007, p. 1.
[33] P. Frugier, S. Gin, J.E. Lartigue, E. Deloule, SON68 glass dissolution kinetics at high reaction progress: mechanisms accounting for the residual alteration rate, in: Mat. Res. Soc. Symp. Proc. vol. 932, 2006, p. 305.
[34] Z. Boksay, G. Bouquet, S. Dobos, Phys. Chem. Glasses 9 (1968) 69.
[35] S. Gin, C. Jegou, Limiting mechanisms of borosilicate glass alteration kinetic:effect of glass composition, in: A.A. Balkema (Ed.), Water–Rock Interaction, first ed., Villasimius, Italy, 2001, p. 279.
[36] I.S. Muller, S. Ribet, I.L. Pegg, S. Gin, P. Frugier, Characterization of alteration phases on HLW glasses after 15 years of PCT leaching, Ceram. Trans., vol. 176, Am. Ceram. Society, Westerville, OH, 2006, p. 191.
[37] M. Aertsens, The BRAG and GM2003 models for glass dissolution, in Mater. Res. Soc. Symp. Proc., vol 985, 2007, p. 117.